DEUTSCHES ELEKTRONEN-SYNCHROTRON DESY

DESY SR-82-08
June 1982

VUV PHOTOABSORPTION AND PHOTOEMISSION OF ATOMIC Cr

by

R. Bruhn, E. Schmidt, H. Schröder and B. Sonntag

II. Institut für Experimentalphysik der Universität Hamburg
and Deutsches Elektronen-Synchrotron DESY, Hamburg

NOTKESTRASSE 85 · 2 HAMBURG 52

To be sure that your preprints are promptly included in the
HIGH ENERGY PHYSICS INDEX ,
send them to the following address (if possible by air mail) :

DESY
Bibliothek
Notkestrasse 85
2 Hamburg 52
Germany

DESY SR-82-08
June 1982

VUV Photoabsorption and Photoemission of Atomic Cr

R. Bruhn, E. Schmidt, H. Schröder and B. Sonntag
II. Institut für Experimentalphysik der Universität Hamburg and
Deutsches Elektronen-Synchrotron DESY, 2000 Hamburg 52, Germany

Abstract

The photoabsorption and photoemission of atomic Cr have been obtained in the photon energy range 30 eV to 70 eV. At the 3p threshold the spectrum is dominated by $3p^6\ 3d^5\ 4s\ (^7S) \rightarrow 3p^5\ 3d^5\ 4s^2\ (^7P)$, $3p^5 3d^6\ 4s\ (^7F, ^7D, ^7P)$ transitions giving rise to discrete absorption lines and a broad asymmetric absorption band. In contrast to the higher Z members of the 3d transition metal series the Cr 3p absorption spectrum shows three well developed $3p^6\ 3d^5\ 4s \rightarrow 3p^5\ 3d^5\ 4s\ nd$ Rydberg series converging towards the $3p^5\ 3d^5\ 4s\ ^8P_{5/2,\ 7/2,\ 9/2}$ states of Cr II. The $3d^4\ 4s\ ^6D$ and $3d^5\ ^6S$ photoemission lines are strongly enhanced above the 3p threshold. As a function of photon energy the intensity of the $3d^5\ ^6S$ line shows a symmetric profile, whereas the $3d^4\ 4s\ ^6D$ line is clearly asymmetric, thus corroborating the interference between 3p and 3d excitations. Asymmetric profiles are also displayed by the two $3d^4\ 4p\ ^6F$, $3d^4\ 5s\ ^6D$ photoemission lines.

To be published in Journal of Physics B

1. Introduction

Cr occupies an important position in the 3d transition metal series. In the $3d^5\ 4s\ ^7S$ ground state the 3d shell is half-filled, whereas the 4s shell, an exception in this series, is incomplete. According to theoretical calculations (Combet-Farnoux 1974), the character of the 3p absorption spectra changes at Cr. For Sc, Ti and V, the $3p^6\ 3d^n \rightarrow 3p^5\ 3d^{n+1}$ oscillator strength is expected to extend over an approximately 10 eV wide band. For Mn, Fe, Co and Ni the $3p^6\ 3d^n \rightarrow 3p^5\ 3d^{n+1}$ oscillator strength is concentrated in a several eV wide strongly asymmetric absorption band (Connerade et al., 1976; Bruhn et al., 1978, 1979). These experimental results agree with the results of calculations based on interaction between the $3p^6\ 3d^n \rightarrow 3p^5\ 3d^{n+1}$ and the $3p^6\ 3d^n \rightarrow 3p^6\ 3d^{n-1}$ ef transitions (Davis and Feldkamp 1976, 1978; Combet Farnoux and Ben Amar 1980). Due to the considerable experimental difficulties there are no experimental 3p spectra of atomic Sc, Ti and V.

The available data on the solid transition metals series Ti to Ni (Sonntag et al., 1969; Wehenkel and Gauthé, 1974) show the Z-dependence of the 3p spectra discussed above. The 3p spectra of atomic Cr reported by Mansfield (1977) seem to indicate that the change occurs between Cr and Mn. Based on Hartree-Fock calculations Mansfield (1977) positioned the main 3p - 3d oscillator strength approximately 10 eV above threshold and 3 eV above the lowest $3p^5\ 3d^5\ 4s\ ^8P$ ionisation limit. Due to the low contrast of these spectra taken photographically there is no clear evidence for a strong absorption band in this region, but as in Mn there is a broad absorption band below the lowest ionisation limit. In order to clarify this and to gain further insight in the coupling of the 3p and 3d excitation, we determined the photoabsorption and the photoemission spectra of atomic Cr for photon energies between 30 eV and 70 eV.

2. Experiment

For the absorption measurements, atomic Cr was maintained inside a resistance heated tubular furnace mounted in front of a 2 m grazing incidence Rowland type spectrograph. To prevent alloying Cr was contained in an aluminium oxide tube. The temperature ranged from 1600° C to 1750° C, which according to vapour pressure data corresponds to pressure between 0.7 and 4 mbar. The

length of the vapour column was ∿ 50 cm. 400 - 600 Å thin Al windows separated the vapour region from the high vacuum of the beam pipe and the spectrograph. Kr or Xe buffer gas (3 - 5 mbar) prevented the metal atoms from reaching the windows. The windows and the buffer gas also effectively served to suppress higher order background. The synchrotron radiation of the electron synchrotron DESY transmitted through the vapour column was focussed on the entrance slit of the spectrograph. The spectra were recorded on photographic plates. The spectrograph was calibrated by means of the known absorption lines of the buffer gases (Codling and Madden 1965, King et al., 1977). The absorption spectra of Kr, Xe and Cr were recorded under identical setting of the optics on adjoining zones (Kr upper and lower zone, Xe and Cr center zone) on the same photographic plate. The Kr 3d absorption lines in second order overlap the sharp Cr 3p absorption lines. The energy positions of the Xe 4d lines, the Kr 3d lines in first and second order could be described by the spectrograph dispersion curve with an accuracy of ± 4 meV. The energy resolution at the 3p-threshold was 10 - 20 meV. From a series of plates obtained under different conditions (vapour pressure, exposure time, windows, buffer gas) the relative spectral dependence of the absorption coefficient has been established.

For the photoemission measurements the synchrotron radiation emitted by the storage ring DORIS was monochromatized (bandwidth 0.1 eV at 30 eV and 0.35 eV at 70 eV) with a new toroidal grating monochromator. The monochromatic photon beam was focussed onto the interaction zone where it crossed a beam of atomic Cr emanating from a resistively heated high temperature furnace (T = 1300 ^{o}C). The kinetic energy of electrons emerging from the interaction zone was determined by a cylindrical mirror analyzer (angular acceptance 0.8% of 4π, energy resolution ΔE = 0.8% of the pass energy). Only electrons emitted at the magic angle of 54^{o} 44' relative to the polarization vector of the incoming light were accepted by the analyzer. This eliminates the asymmetry of the photoelectron angular distribution (Starace 1982) and allows for a direct determination of partial cross-sections. All photoemission spectra were normalized to the incoming photon flux and corrected for the energy dependent dispersion of the electron analyzer. Since the density of atoms in the interaction zone was not determined, only relative cross-sections are given. Details of the experimental set-up will be presented elsewhere (Bruhn et al., 1982a).

3. Results and Discussion

The 3p absorption spectrum of atomic Cr is presented in Figure 1. In order to get the zero, the spectrum of atomic Cr has been normalized to that of metallic Cr below the 3p threshold. For comparison, the densitometer trace reported by Mansfield (1977) is given. Note that the energies of the absorption

lines given by Mansfield (1977) are too low by 0.6 - 0.8 eV. At the 3p threshold there are three prominent lines (Nos. 1 - 3, see Fig. 1) which, in agreement with Mansfield, we ascribe to $3p^6\ 3d^5\ 4s\ ^7S_3 \rightarrow 3p^5\ 3d^5\ 4s^2\ ^7P_{2,3,4}$ transitions. Towards higher photon energies, there is a series of very weak lines (Nos. 4 - 11) followed by a prominent doublet (Nos. 12, 13). The dominant feature of the spectrum is a broad absorption band (No. 17) centered at 43.8 eV. Absorption lines are superimposed on this broad band on both sides of the maximum (Nos. 14 - 16, 17 - 22).

Three well-developed Rydberg series show up above 44 eV. This part of the spectrum is presented on an enlarged scale in Figure 2. The strong asymmetric lines belong to $3p^6\ 3d^5\ 4s \rightarrow 3p^5\ 3d^5\ 4s\ nd$ series converging to the series limits $3p^5\ 3d^5\ 4s\ ^8P_{9/2}$ (46.365 ± 0.01 eV), $^8P_{7/2}$ (46.725 ± 0.01 eV) and $^8P_{5/2}$ (47.050 ± 0.01 eV). The splitting of these series limits is in good agreement with HF-values reported by Mansfield (1977) $^8P_{9/2}$ (43.756 eV), $^8P_{7/2}$ (44.143 eV), $^8P_{5/2}$ (44.443), but these calculated absolute values are 2.6 eV too low. The experimental series limits given above and quantum defects of 0.88, 0.82 and 0.81 allow a good approximation of the energy positions of the higher members of the Rydberg series. These values for the quantum defects are in good agreement with those expected for nd series. We ascribe the sharp absorption lines in this energy range (e.g. Nos. 18-23, 27, 28, 30, 31, 33, 34, 38, 39) to $3p^6\ 3d^5\ 4s \rightarrow 3p^5\ 3d^5\ 4s\ ns$ series converging towards the same series limits. It is interesting to note that the members of these series (Nos. 18-22) superimposed on the sloping background of the broad absorption band clearly show asymmetric Fano type line shapes. The quantum defect of these ns series is ∿2.5. In Figure 1 we see above the ^8P series limits weak absorption lines (Nos. 80-97) sitting on a big continuous background. Rydberg series converging towards higher series limits and two electron excitations are responsible for these lines.

Now let us return to the structures between 40 eV and 44.5 eV (Nos. 4-17) which we skipped in our assignment. We expect $3p^6\ 3d^5\ 4s \rightarrow 3p^5\ 3d^6\ 4s$ transitions to prevail in this region. Except for the missing 4s electron, this is very similar to the $3p^6\ 3d^5\ 4s^2 \rightarrow 3p^5\ 3d^6\ 4s^2$ excitation in atomic Mn (Bruhn et al., 1978). Transferring the interpretation of the corresponding

part of the Mn spectrum to the spectrum of Cr results in the following assignment: The broad band (No. 17) centered at 43.8 eV is due to $3p^6\ 3d^5\ 4s\ ^7S_3 \rightarrow 3p^5\ (3d^6\ ^5D)\ 4s\ ^7P_{2,3,4}$ transitions. If, as in Mn, LS-coupling dominates and the $3p^5\ 3d^5\ 4s$ ground state electrons remain spectators, these transitions should have the largest oscillator strength. The width and lineshape of this band is caused by the interference of the $3p^6\ 3d^5\ 4s\ ^7S \rightarrow 3p^5\ 3d^6\ 4s\ ^7P$ and the $3p^6\ 3d^5\ 4s\ ^7S \rightarrow 3p^6\ 3d^4\ (^5D)\ 4s\ \varepsilon f\ ^7P$ mediated via the super-Coster Kronig decay $3p^5\ 3d^6\ 4s\ ^7P \rightarrow 3p^6\ 3d^4\ 4s\ \varepsilon f\ ^7P$. Deviations from LS coupling due to the spin orbit splitting of the 3p core give rise to weak intercombination lines $3p^6\ 3d^5\ 4s\ ^7S \rightarrow 3p^5\ 3d^6\ 4s\ ^7D, ^7F$. As for $3p^5\ 3d^6\ 4s^2\ ^6D$ in Mn the decay of the Cr $3p^5\ 3d^6\ 4s\ ^7D$ states into $3p^6\ 3d^4\ 4s\ \varepsilon f\ ^7D$ is forbidden by selection rules. Therefore in analogy to Mn we assign the sharp lines at 42.229 eV (No. 12) and 42.322 eV (No. 13) to transitions to $3p^5\ 3d^6\ 4s\ ^7D$ states. The oscillator strength of the transitions to the $3p^5\ 3d^6\ 4s\ ^7F$ states is very small and they are only weakly affected by the super-Coster Kronig decay. We tentatively assign the lines at 41.677 eV (No. 9); 41.775 eV (No. 10) and 41.913 eV (No. 11) to these transitions. Our assignments consistent with the spectator model are summarized in Table 1.

Based on his Hartree-Fock calculations Mansfield expected the $3p^5\ 3d^6\ 4s\ ^7P$ state at 47.262 eV, i.e. above the $3p^5\ 3d^5\ 4s\ ^8P$ ionisation limits. Our spectra do not show any strong absorption band in this spectral range. Due to the neglection of correlation effects Hartree-Fock calculations tend to overestimate the multiplet splitting. For Mn Connerade et al. (1976) calculated a splitting between $3p^5\ 3d^6\ 4s^2\ ^6F$ and $3p^5\ 3d^6\ 4s^2\ ^6P$ of 6 eV which overshoots the experimental value by 3 eV. Subtracting 3 eV from the splitting between the $3p^5\ 3d^6\ 4s\ ^7F$ (41.6 eV) and the $3p^5\ 3d^6\ 4s\ ^7P$ (47.3 eV) brings the ^7P level down to 44.3, which is very close to the experimental value (43.80 eV). Furthermore, the energy of the ^7P resonance will be shifted from the Hartree-Fock value due to the interaction with the continua. For Mn Davis and Feldkamp (1978) obtained - 2 eV for this shift.

In Figure 3 the photoemission spectrum of atomic Cr taken at 43.6 eV is shown. Line number 3, corresponding to the $3p^6\ 3d^4\ (^5D)\ 4s\ ^6D$ state of CrII, dominates the spectrum. The weaker line (4) at lower binding energies is due to the emission of the 4s electron. Two shake-up satellite lines (1,2) show up at higher binding energies. The experimentally determined binding energies and our assignment, which is based on the published energy

level data (Sugar and Corliss, 1977), are presented in Table 2. To check the validity of the interpretation of the absorption spectrum given above, it is crucial to determine the intensity of the dominant photoemission line as a function of the photon energy. In analogy to Mn (Bruhn et al., 1982b) we expect an asymmetric Fano-type line shape caused by the interference of the

$$3p^6\ 3d^5\ 4s\ ^7S \rightarrow 3p^5\ 3d^6\ 4s\ ^7P \quad \text{and the} \quad 3p^6\ 3d^5\ 4s\ ^7S \rightarrow 3p^6\ 3d^4\ 4s\ \varepsilon\ell\ ^7P$$

excitations. This expectation is clearly verified by the asymmetric line shape presented in Figure 4. Note that experimental data in the regions of the Rydberg series (44.5 eV - 47.5 eV) and $3p^6\ 3d^5\ 4s\ ^7S \rightarrow 3p^5\ 3d^5\ 4s^2\ ^7P$ excitations are not included in Figure 4. The experimental points can be approximated by a Fano type line shape (Fano and Cooper, 1968)

$$\sigma = \frac{(\varepsilon + q)^2}{1 + \varepsilon^2} \quad \text{with} \quad \varepsilon = \frac{E - E_0}{1/2\ \Gamma}$$

The energy of the resonance E_0, the line width Γ and the asymmetry parameter q giving the best fit to the experimental data are included in Figure 4. The q value of 3.1 is somewhat larger than the value of 2.3 obtained for Mn. The line width (Γ = 0.75 eV) is almost a factor 2 smaller than the corresponding line width for Mn (Γ = 1.3 eV) (Bruhn et al., 1982b).

The almost constant photoemission intensity above the $^8P_{5/2}$ ionisation limit excludes the existence of the strong $3p^6\ 3d^5\ 4s^7\ S \rightarrow 3p^5\ 3d^6\ 4s\ ^7P$ resonance band in this energy range. The deviation of experimental points from the theoretical curve between 42 - 43 eV is caused by the decay of the $3p^5\ 3d^6\ 4s\ ^7D_{2,3,4}$ and $3p^5\ 3d^6\ (^4P)\ 4s$ states into $3p^6\ 3d^4\ 4s\ (^6D)\ \varepsilon\ell$. Again this is similar to the situation for atomic Mn (Bruhn et al., 1982). The intensity of the $3d^4\ 4s\ (^6D)$ photoemission line replicates the $3p^6\ 3d^5\ 4s\ ^7S \rightarrow 3p^5\ 3d^5\ 4s^2\ ^7P_{2,3,4}$ absorption lines. This proves the importance of the $3p^5\ 3d5\ 4s2\ 7P \rightarrow 3p6\ 3d4\ 4s\ \varepsilon\ell\ ^7P$ Coster Kronig decay and explains the considerable line width of the absorption lines (1-3)(FWHM = 0.2 eV). The asymmetric Fano-type line shape of the $3p^5\ (3d^5\ ^6S)\ (^7P)\ 4s\ ^8P$ nd Rydberg lines manifests the coupling to the underlying continua. This is borne out by the photoemission results presented in Figure 5. The intensity of the $3p^5\ 3d^4\ 4s\ (^6D)$ photoemission line closely follows the absorption spectrum. In order to facilitate the comparison the absorption spectrum has been convoluted with a Gaussian distribution of 0.15 eV width, thus taking the lower resolution of the toroidal grating monochromator into account.

The intensity of the $3p^6\ 3d^5\ ^6S$ photoemission line versus photon energy is presented in Figure 6. Also this line is strongly enhanced at the energy of the $3p^6\ 3d^5\ 4s\ ^7S \rightarrow 3p^5\ 3d^6\ 4s\ ^7P$ transition. Neglecting the deviations due to the coupling to the $3p^5\ 3d^5\ 4s^2\ ^7P$, $3p^5\ 3d^6\ 4s\ ^6D$ and $3p^5\ 3d^6\ (^4X)\ 4s$ lines, the line shape can be approximated by a symmetric Lorentzian curve. The line is mainly driven by the $3p^5\ 3d^6\ 4s\ ^7P \rightarrow 3p^6\ 3d^5\ \varepsilon\ell\ ^7P$ Auger transition. Interference effects can be neglected due to the small oscillator strength of the $3p^6\ 3d^5\ 4s \rightarrow 3p^6\ 3d^5\ \varepsilon\ell$ transitions. Interference effects are not negligible for the $3p^5\ 3d^4\ (^5D)\ 5s\ ^6D$ and $3p^5\ 3d^4\ (^5D)\ 4p\ ^6D$ photoemission lines which exhibit asymmetric line shapes. They mainly originate from the decay of the $3p^5\ 3d^6\ 4s\ ^7P$ state to $3p^6\ 3d^4\ (^5D)\ 4p\ ^6D\ \varepsilon\ell$ and $3p^6\ 3d^4\ (^5D)\ 5s\ ^6D$, respectively. Their intensity as function of photon energy follows the intensity variation of the $3p^6\ 3d^4\ 4s\ ^6D$ line. This behavior agrees with the results for similar shake-up satellite lines for atomic Mn (Bruhn et al., 1982b).

Acknowledgment

The authors thank H.E. Wetzel for his help in performing the measurements.

References

Bruhn, R., Sonntag, B. and Wolff, H.W., 1978, Phys. Lett. 69A, 9.

Bruhn, R., Sonntag, B. and Wolff,H.W., 1979, J.Phys.B: Atom Molec. Phys. 12, 203.

Bruhn, R., Schmidt E., Schröder, H. and Sonntag, B., 1982a. Proc. Int. Conf. on X-ray and VUV Synchrotron Radiation Instrumentation, Nuclear Instruments and Methods (to be published).

Bruhn, R., Schmidt, E., Schröder, H. and Sonntag, B., 1982b, submitted to Phys. Lett. A.

Codling, K. and Madden, R.P., 1965, Appl. Opt. 4, 1431.

Combet-Farnoux, F., 1974, Physica Fennica 9, Suppl. S1, 80.

Combet-Farnoux, F. and Ben Amar, M., 1980, Phys. Rev. A21, 1975.

Connerade, J.P., Mansfield M.W.D. and Martin, M.A.P., 1976, Proc. R. Soc. Lond. A350, 405.

Davis, L.C. and Feldkamp, L.A., 1976, Solid State Commun. 19, 413.

Davis, L.C. and Feldkamp, L.A., 1978. Phys. Rev. A17, 2012.

Fano, U. and Cooper, J.W., 1968, Rev. Mod. Phys. 40, 441.

King, G.C., Tronc, M., Read, F.H. and Bradford, R.C., 1977, J. Phys. B: Atom. Molec. Phys. 10, 2479.

Mansfield, M.W.D., 1977, Proc. Roy. Soc. Lond. A358, 253.

Sonntag, B., Haensel, R. and Kunz, C., 1969, Solid State Commun. 7, 597.

Starace, A.F., 1982, Theory of Atomic Photoionization in: Handbuch der Physik, Vol. 31 (to be published)

Sugar, J. and Corliss, Ch., 1977, Journal of Physics and Chemical Reference Data 6, 317.

Wehenkel, C. and Gauthe, B., 1974, Phys. Lett. 47A, 253 and Phys. Stat. Sol. B64, 515.

Figure Captions

Figure 1 — 3p-photoabsorption spectrum of atomic Cr (solid line). For comparison the densitometer curve reported by Mansfield (1976) is included (dashed line).

Figure 2 — 3p-photoabsorption of atomic Cr in the region of the $3p^6\ 3d^5\ 4s\ ^7S \rightarrow 3p^5\ (3d^5\ ^6S)\ (^7P)\ 4s\ ^8P$ ns, nd Rydberg series.

Figure 3 — Photoemission spectrum of atomic Cr taken at 43.6 eV.

Figure 4 — Experimentally determined intensity of the Cr $3p^6\ 3d^4\ 4s\ ^6D$ photoemission line for photon energies between 25 eV and 70 eV (•). No data are given in the region of the ^7P excitations (39-40 eV) and the Rydberg series (44.5-47 eV). The experimental data are approximated by a Fano type line shape (——).

Figure 5 — Experimentally determined intensity of the Cr $3p^6\ 3d^4\ 4s\ ^6D$ photoemission line in the region of the $3p^6\ 3d^5\ 4s\ ^7S \rightarrow 3p^5\ (3d^5\ ^6S)\ (^7P)\ 4s\ ^8P$ ns, nd Rydberg series (•). The solid curve gives the absorption spectrum convoluted by a Gaussian curve of 0.15 eV width.

Figure 6 — Experimentally determined intensity of the Cr $3p^6\ 3d^5\ ^6S$ photoemission line for photon energies between 35 eV and 50 eV (•). The experimental data are approximated by a Lorentzian curve (——).

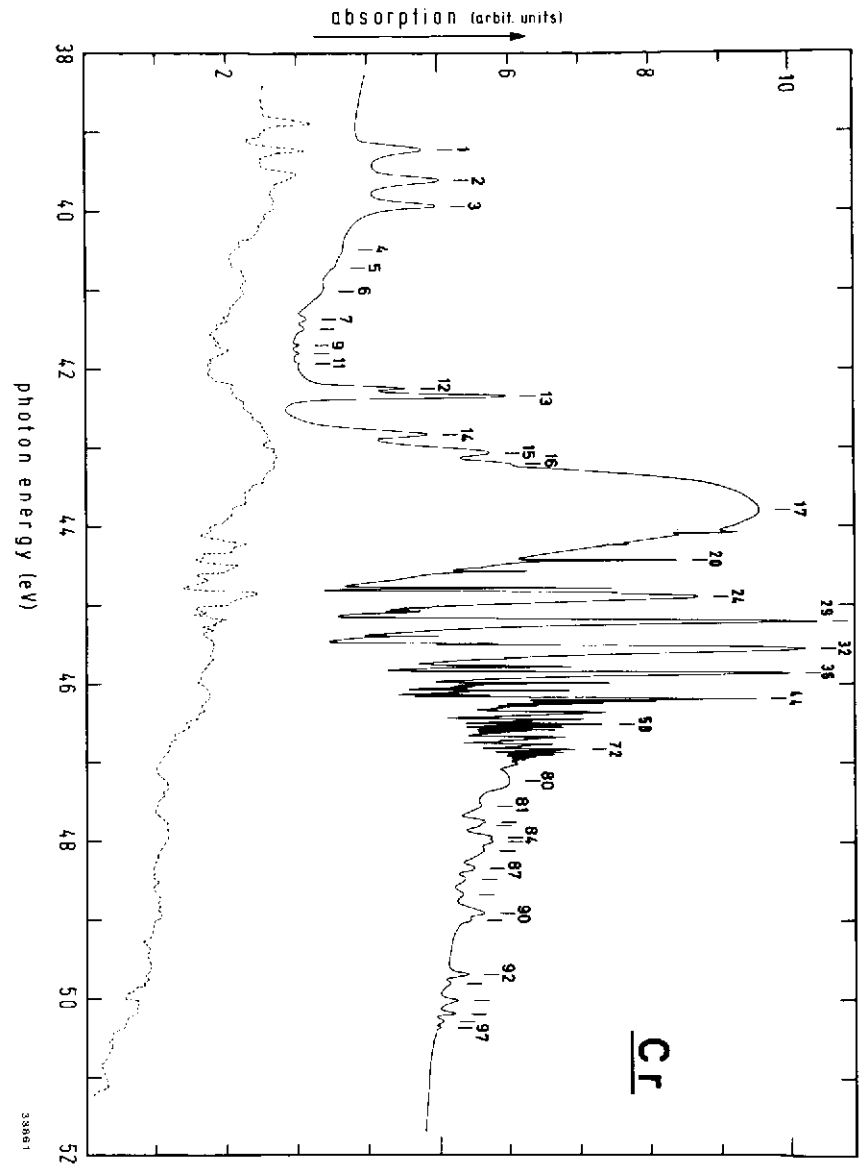

Fig. 1

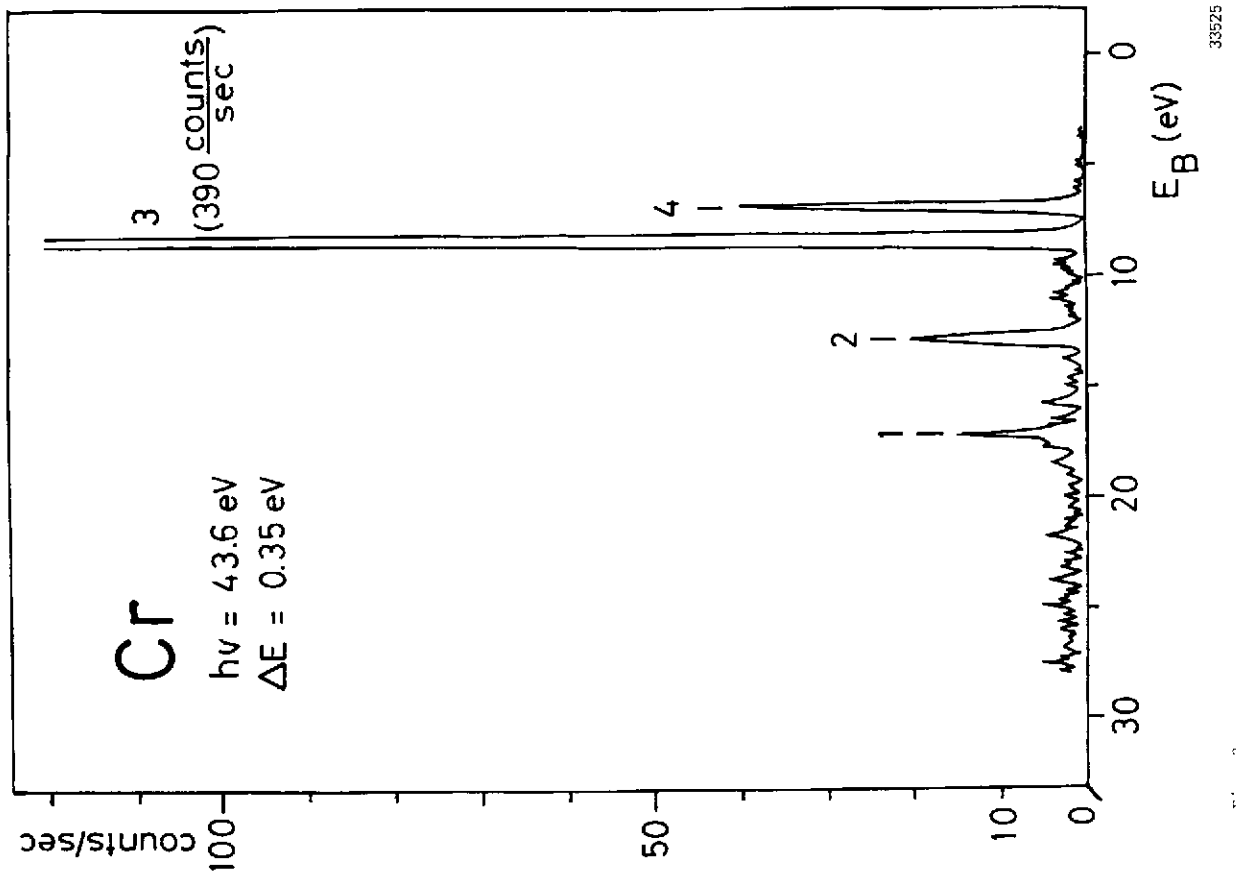
Cr
hν = 43.6 eV
ΔE = 0.35 eV
3
(390 counts/sec)
4
1
2
counts/sec
100
50
10
0
0
10
20
30
E_B (eV)
33525

Fig. 3

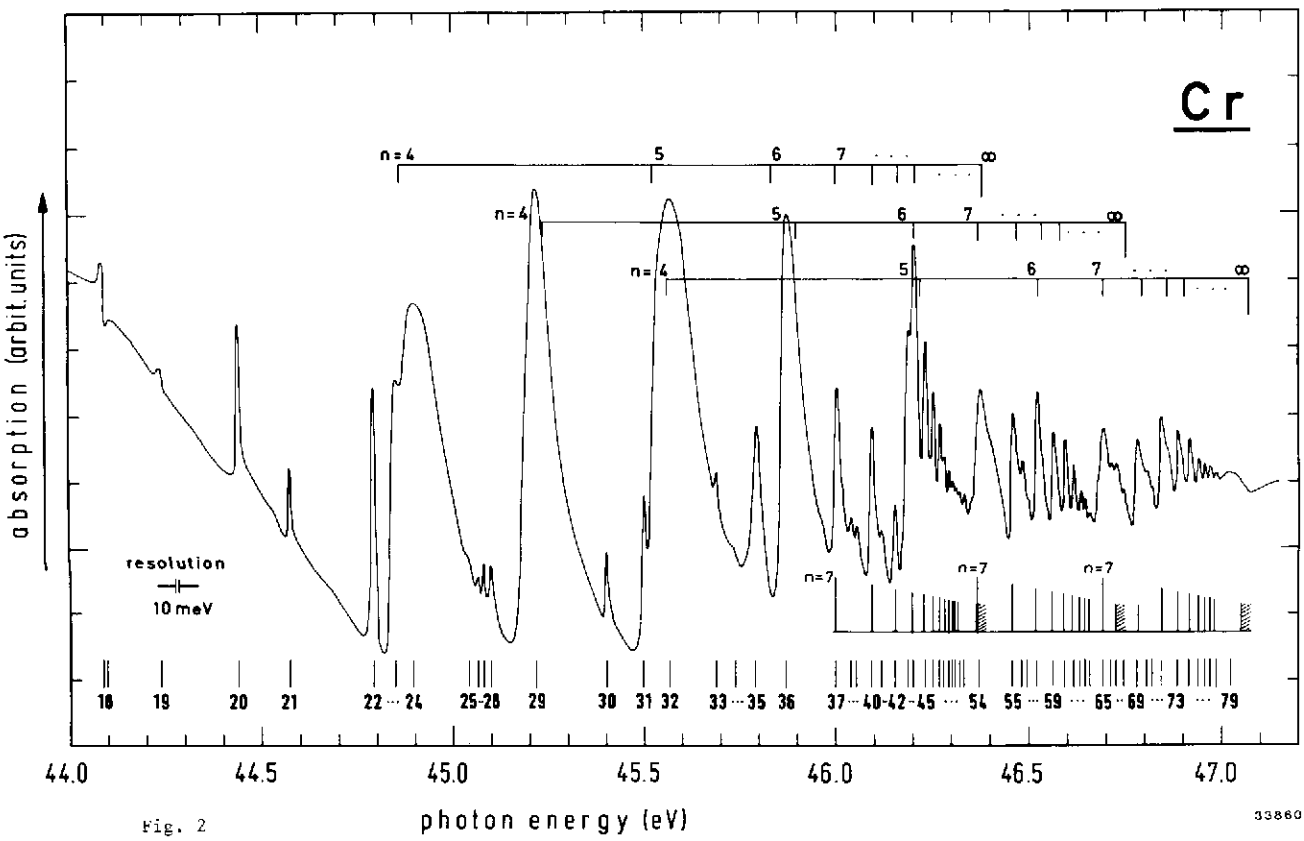
Cr
absorption (arbit.units)
resolution
10 meV
n=4
5
6
7
8
n=7
18
19
20
21
22 ··· 24
25-28
29
30
31 32
33 ··· 35 36
37 ··· 40-42-45 ··· 54
55 ··· 59 ··· 65 ··· 69 ··· 73 ··· 79
44.0
44.5
45.0
45.5
46.0
46.5
47.0
photon energy (eV)
33860

Fig. 2

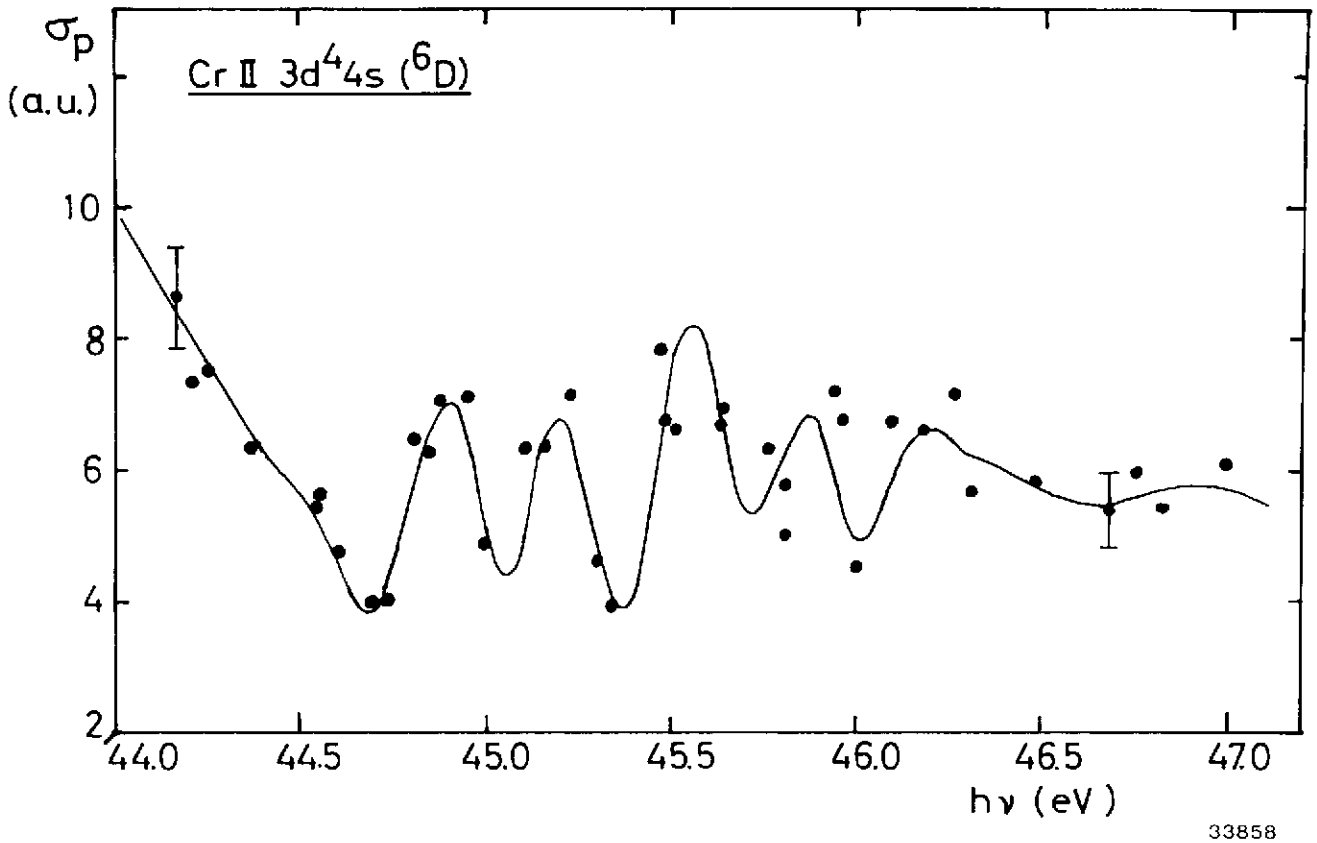
σp
(a.u.)
Cr II 3d⁴4s (⁶D)
10
8
6
4
2
44.0
44.5
45.0
45.5
46.0
46.5
47.0
hν (eV)
33858

Fig. 5

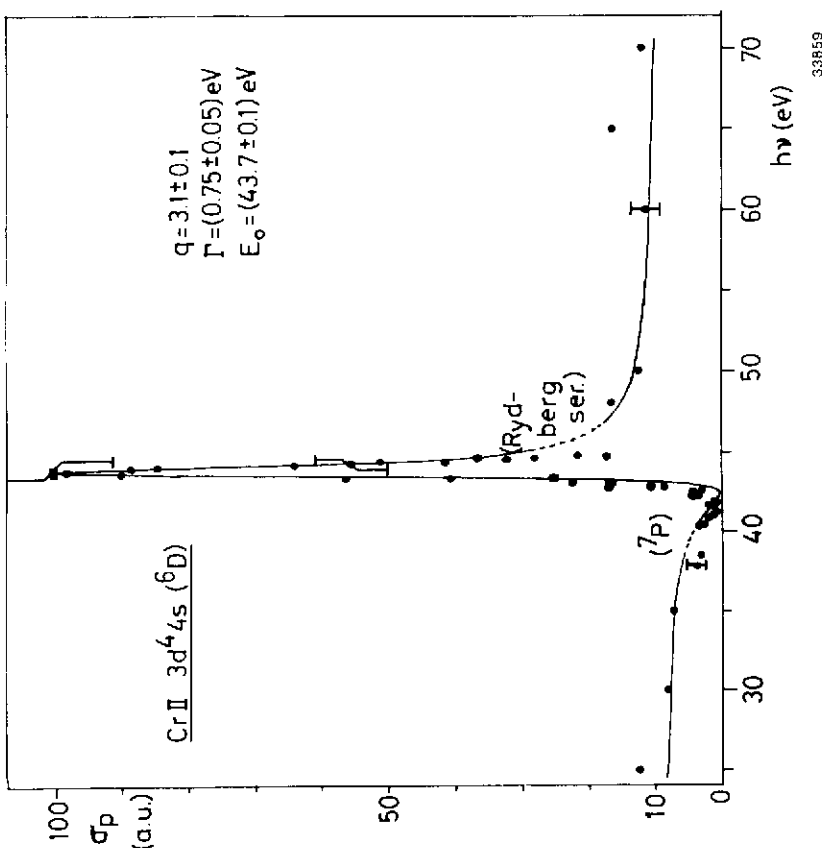
q=3.1±0.1
Γ=(0.75±0.05) eV
E₀=(43.7±0.1) eV
Ryd-
berg
ser.)
(⁷P)
Cr II 3d⁴4s (⁶D)
σp (a.u.)
100
50
10
0
70
60
50
40
30
hν (eV)
33859

Fig. 4

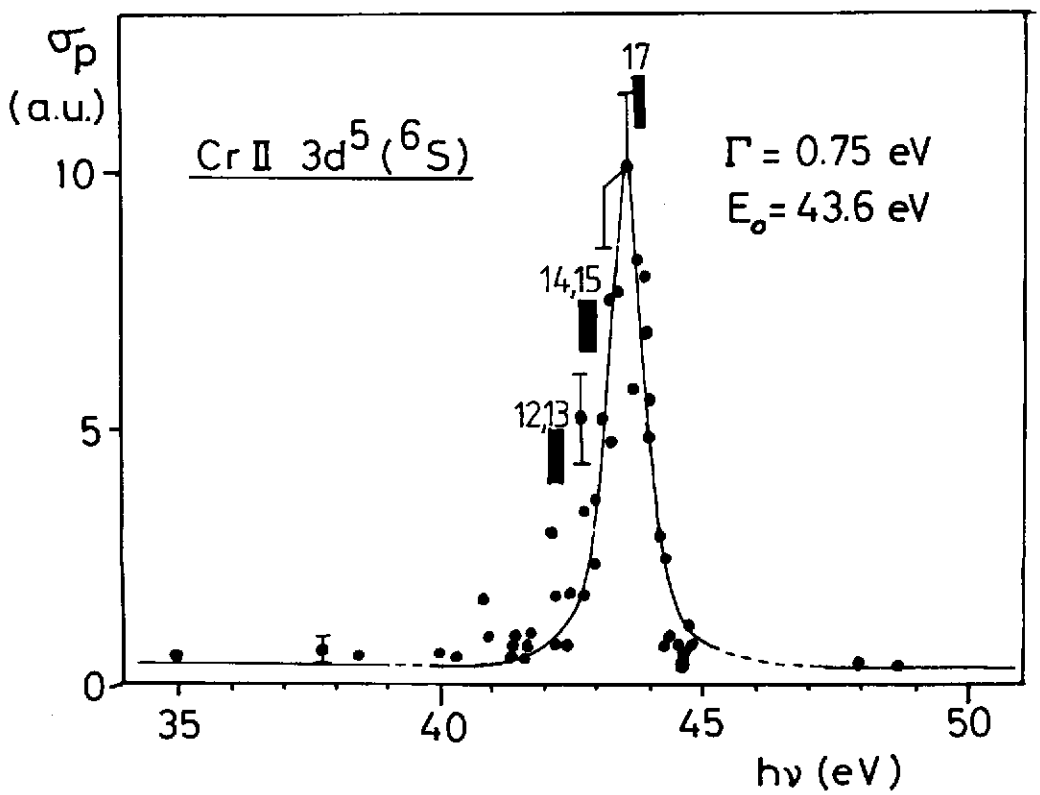
σp
(a.u.)
10
5
0
Cr II 3d5 (6S)
17
14,15
12,13
Γ = 0.75 eV
Eo = 43.6 eV
35
40
45
50
hν (eV)

Fig. 6

33857

Table 1: Observed CrI absorption lines with assignments.
The numbers in brackets denote the uncertainty of the last digits of each energy value. The whole spectrum may be shifted by ± 0.04 eV.

line No. (see Figs. 1 and 2)	energy (eV)		assignment (upper level)
1	39.207	(8)	$3p^5\ 3d^5\ 4s^2\ {}^7P_4$
2	39.588	(8)	$3p^5\ 3d^5\ 4s^2\ {}^7P_3$
3	39.909	(8)	$3p^5\ 3d^5\ 4s^2\ {}^7P_2$
4	40.487	(25)	
5	40.717	(33)	
6	41.020	(50)	
7	41.351	(25)	
8	41.461	(17)	
9	41.677	(10)	$3p^5\ 3d^6\ 4s\ {}^7F_4$
10	41.775	(10)	$3p^5\ 3d^6\ 4s\ {}^7F_3$
11	41.913	(10)	$3p^5\ 3d^6\ 4s\ {}^7F_2$
12	42.229	(5)	$3p^5\ 3d^6\ 4s\ {}^7D_{2,3,4}$
13	42.322	(3)	
14	42.804	(3)	$3p^5\ 3d^6\ ({}^4P)\ 4s$
15	43.042	(7)	
16	43.205	(8)	
17	43.80	(5)	$3p^5\ 3d^6\ 4s\ {}^7P_{2,3,4}$
18	44.093	(6)	$3p^5\ (3d^5\ {}^6S)\ ({}^7P)\ 4s\ {}^8P_{9/2}\ 5s$
19	44.239	(5)	
20	44.439	(13)	" " $^8P_{7/2}$ 5s
21	44.574	(13)	
22	44.791	(8)	" " $^8P_{5/2}$ 5s
23	44.849	(2)	
24	44.896	(5)	" " $^8P_{9/2}$ 4d
25	45.043	(3)	
26	45.065	(2)	" " $^8P_{9/2}$ 6s
27	45.081	(2)	
28	45.099	(2)	
29	45.217	(2)	" " $^8P_{7/2}$ 4d
30	45.401	(1)	" " $^8P_{7/2}$ 6s
31	45.498	(1)	

(TABLE 1)

line No. (see Figs. 1 and 2	energy (eV)		assignment (upper level)
32	45.566	(3)	$3p^5\ (3d^5\ {}^6S)\ ({}^7P)\ 4s\ {}^8P_{9/2}$ 5d; " " $^8P_{5/2}$ 4d
33	45.688	(2)	" " $^8P_{5/2}$ 6s
34	45.740	(5)	
35	45.790	(2)	" " $^8P_{9/2}$ 6d
36	45.870	(2)	" " $^8P_{7/2}$ 5d
37	46.000	(2)	" " $^8P_{9/2}$ 7d
38	46.038	(2)	" " $^8P_{7/2}$ 7s
39	46.052	(2)	
40	46.092	(2)	" " $^8P_{9/2}$ 8d
41	46.118	(2)	
42	46.154	(2)	" " $^8P_{9/2}$ 9d
43	46.187	(2)	" " $^8P_{9/2}$ 10d; $^8P_{7/2}$ 6d; $^8P_{5/2}$ 5d
44	46.200	(2)	
45	46.231	(2)	" " $^8P_{9/2}$ 11d
46	46.251	(2)	" " " 12d
47	46.269	(2)	" " " 13d
48	46.280	(2)	" " " 14d
49	46.293	(2)	" " " 15d
50	46.302	(2)	" " " 16d
51	46.311	(2)	" " " 17d
52	46.322	(2)	" " " 18d
53	46.333	(2)	
54	46.372	(2)	" " $^8P_{7/2}$ 7d
55	46.457	(2)	" " $^8P_{7/2}$ 8d
56	46.482	(2)	
57	46.497	(2)	
58	46.520	(2)	" " $^8P_{5/2}$ 6d; $^8P_{7/2}$ 9d
59	46.564	(2)	" " " 10d
60	46.593	(2)	" " " 11d
61	46.617	(2)	" " " 12d
62	46.634	(2)	" " " 13d
63	46.647	(2)	" " " 14d
64	46.658	(2)	" " " 15d

(TABLE 1)

line No. (see Figs. 1 and 2	energy (eV)		assignment (upper level)
65	46.693	(2)	$3p^5$ ($3d^5$ ^6S) (^7P) 4s $^8P_{5/2}$ 7d
66	46.712	(2)	
67	46.725	(2)	
68	46.745	(2)	
69	46.779	(2)	" " " 8d
70	46.805	(2)	
71	46.818	(2)	
72	46.842	(2)	" " " 9d
73	46.885	(2)	" " " 10d
74	46.915	(2)	" " " 11d
75	46.938	(2)	" " " 12d
76	46.956	(2)	" " " 13d
77	46.969	(2)	" " " 14d
78	46.986	(3)	" " " 15d
79	47.02	(2)	
80	47.26	(2)	
81	47.56	(2)	
82	47.76	(1)	
83	47.81	(2)	
84	47.96	(1)	
85	48.01	(1)	
86	48.13	(2)	
87	48.35	(1)	
88	48.48	(2)	
89	48.68	(1)	
90	48.92	(1)	
91	49.02	(2)	
92	49.70	(1)	
93	49.82	(1)	
94	50.03	(1)	
95	50.20	(2)	
96	50.29	(2)	
97	50.38	(2)	

TABLE 2

Experimental binding energies E_B of the states of CrII giving rise to the photoemission lines in Fig. 3.

Line	E_B (eV)	State of CrII
1	17.0 ± 0.2	$3p^6$ $3d^4$ (^5D) 5s ^6D
2	12.7 ± 0.2	$3p^6$ $3d^4$ (^5D) 4p ^6F
3	8.2 ± 0.1	$3p^6$ $3d^4$ 4s ^6D
4	6.8	$3p^6$ $3d^5$ ^6S ref.